Lasers and liposomes : a potentially efficacious combination for the non-invasive removal of pathological cutaneous vasculature

Heger, M.

Publication date
2009

7

Tranexamic acid-containing thermosensitive liposomal formulations for antifibrinolytic site-specific pharmaco-laser therapy

MICHAL HEGER
IRENE HAMELERS
JOHAN F. BEEK
THOMAS M. VAN GULIK
BERNARD CHOI
ANTON I.P.M. DE KROON

ABSTRACT

Site-specific pharmaco-laser therapy (SSPLT) is a developmental stage treatment modality designed to non-invasively remove superficial vascular pathologies such as port wine stains (PWS) by combining conventional laser therapy with the prior administration of a prothrombotic and/or antifibrinolytic pharmaceutical-containing drug delivery system. For the antifibrinolytic SSPLT component, six different PEGylated thermosensitive liposomal formulations encapsulating tranexamic acid (TA), a potent antifibrinolytic lysine analogue, were characterized for drug:lipid ratios, encapsulation efficiencies, size, endovesicular TA concentrations (C_{TA}), and phase transition temperature (T_m) and assayed for heat-induced TA release. Assays were developed for the quantification of liposomal TA and heat-induced TA release from two candidate formulations. The outcome parameters were then combined with a 3D histological reconstruction of a port wine stain biopsy to extrapolate in vivo posologies for SSPLT. The prime formulation, DPPC:DSPE-PEG2000 (96:4 molar ratio), had a drug:lipid ratio of 0.82, an encapsulation efficiency of 1.29%, a diameter of 155nm, a C_{TA} of 214mM. The peak TA release from this formulation (T_m=42.3°C) comprised 96% within 2.5min, whereas this was 94% in 2min for DPPC:MPPC:DSPE-PEG2000 (86:10:4) liposomes (T_m=41.5°C). Computational analysis revealed that <400 DPPC:DSPE-PEG2000 (96:4 molar ratio) liposomes are needed to treat a PWS of 40cm^2, compared to a three-fold greater quantity of DPPC:MPPC:DSPE-PEG2000 (86:10:4) liposomes, indicating that, in light of the assayed parameters and endovascular laser-tissue interactions, the former formulation is most suitable for antifibrinolytic SSPLT.

Keywords:
Liposomes, fibrinolysis, fluorescamine derivatization, heat-induced release, drug delivery system, port wine stains

1. INTRODUCTION

Site-specific pharmaco-laser therapy (SSPLT) is a development-stage treatment modality designed to target cutaneous vascular pathologies (e.g., port wine stains) by combining non-invasive laser irradiation with the concomitant systemic administration of prothrombotic and/or antifibrinolytic agents encapsulated in a drug carrier [1]. The intended clinical effect of SSPLT – the removal of aberrant dermal blood vessels – emanates from two principal components of endovascular laser-tissue interactions: the photothermal response and the hemodynamic response. The photothermal response (Fig. 1A-C) entails the conversion of radiant energy to heat by (oxy)hemoglobin and subsequent formation of a thermal coagulum (an amorphous clump of denatured blood) and thermal necrosis of vascular tissue as a result of heat diffusion [2,3]. The hemodynamic response (Fig. 1D-I) refers to the initiation of primary and secondary hemostasis in consequence to the photothermal response, culminating in the formation of a thrombus [4]. Both responses can lead to prolonged cessation of blood flow in case of complete laser-induced occlusion of the vascular lumen (either by a thermal coagulum, a thrombus, or both), triggering chronic inflammatory processes during which the affected vasculature is removed [1]. Unfortunately, in many instances the targeted vascular structures are only partially occluded following laser irradiation [5,6], which has been correlated to suboptimal clinical outcomes [7,8]. SSPLT was therefore introduced to compensate for the incomplete photocoagulation of blood vessels by means of systematically amplifying the hemodynamic response, thereby instilling complete occlusion of the vascular lumen through drug-mediated hyperthrombosis (Fig. 1J-M).

Previously we proposed that tranexamic acid (TA), an antifibrinolytic agent that is widely used in the clinical setting to deter blood loss [9-11] through its antagonistic effect on plasmin(ogen) [12,13], is a drug candidate for the antifibrinolytic component of SSPLT [14]. The chemical simplicity and small size of TA (MW = 157.2) together with its hydrophilicity and high solubility at physiological pH make this molecule suitable for encapsulation into thermosensitive liposomes. Liposomal formulations that make use of thermosensitivity as a drug release mechanism have been widely studied in relation to oncological applications [15-17]. In addition to the "traditional" thermosensitive liposomes composed of diacyl phosphatidylcholines, lysolecithin-containing thermosensitive liposomes have been found to enhance the release kinetics of compounds such as doxorubicin and calcein [15]. Both classes of liposomes may therefore be suitable for SSPLT given the thermal nature of endovascular laser-tissue interactions.

Consequently, six TA-encapsulating liposomal formulations with 1,2-dipalmitoyl-*sn*-glycero-3-phosphocholine (DPPC) as the main component phospholipid were evaluated for their potential applicability in SSPLT. First, an analytical method based on primary amine derivatization with fluorescamine was developed to quantify liposomal encapsulation of TA. Next, TA-encapsulating DPPC liposomes with increasing concentrations 1,2-distearoyl-*sn*-glycero-3-phosphoethanolamine-polyethylene glycol (DSPE-PEG) and lysoPC (1-palmitoyl-2-hydroxy-*sn*-glycero-3-phosphocholine, MPPC) were analyzed for drug:lipid ratio, size, encapsulation efficiency, trapped volume, endovesicular TA concentration, and phase transition temperature (T_m). Finally, an offline drug quantification method was devised to determine the

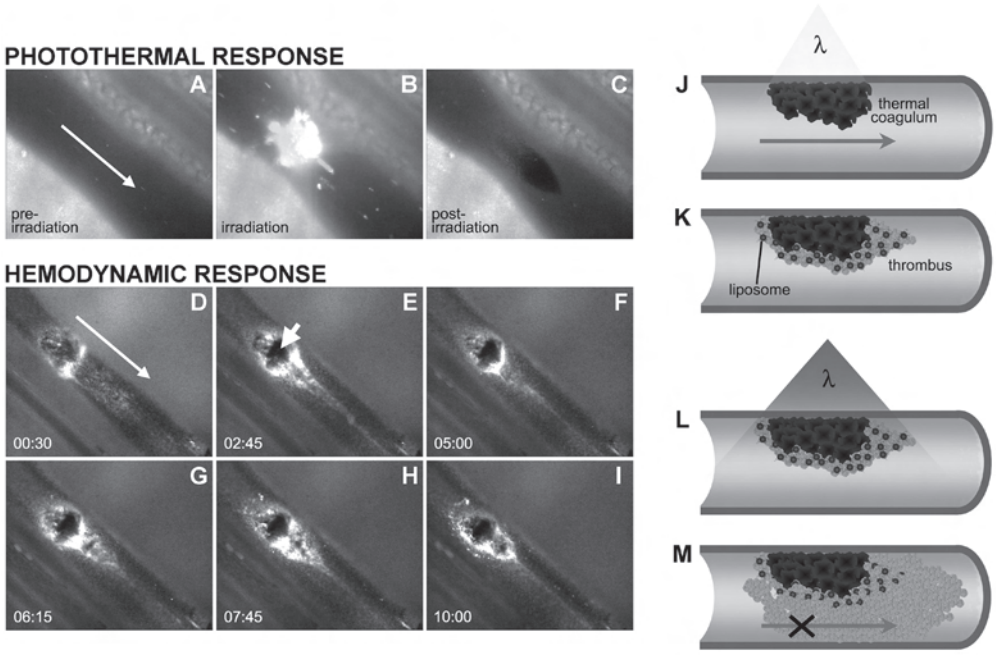

Figure 1. Endovascular laser-tissue interactions and the principles of site-specific pharmaco-laser therapy (SSPLT). The first component of endovascular laser-tissue interactions is the photothermal response (**A-C**), where laser irradiation of a blood vessel ((A), arrow indicates direction of blood flow) with a wavelength predominantly absorbed by hemoglobin results in the formation of a thermal coagulum (C). The photothermal response triggers the hemodynamic response (**D-I**), characterized by platelet aggregation and initiation of the coagulation cascade that culminates in the formation of a thrombus (fluorescently labeled) around the thermal coagulum ((**E**), arrow). The video sequences were recorded in hamster dorsal skin fold venules. Thermal coagula were induced as described in (ref. 3) and thrombi were stained with carboxyfluorescein for visualization by intravital fluorescence microscopy. The elapsed time (min: sec) after the laser pulse is indicated in the lower left corner. The principles of SSPLT (**J-M**) are predicated on both components of endovascular laser-tissue interactions ((J), thermal coagulum and (K), thrombus), whereby the hemodynamic response is systematically amplified by the infusion of a prothrombotic and/or antifibrinolytic agent-containing drug delivery vehicle such as thermosensitive liposomes (K) to instill complete occlusion of the target vessel (M) and subsequent removal of the vessel by the reticuloendothelial system (ref 1). The liposomes can be targeted to the thrombus by liposome-conjugated antibodies directed against epitopes on activated platelets (e.g., CD41, CD62P) or fibrin (K). Following liposome accumulation, drug release can be induced by local heating, e.g., by a second near-infrared laser pulse ((L), lambda). The arrows in (J) and (M) indicate blood flow; the cross out sign in (M) designates cessation of blood flow. Data presented in panels A-I were taken from [4] and M. Heger et al., "Thrombosis as an integral component of endovascular laser-tissue interactions: the fundamental premise for site-specific pharmaco-laser therapy," manuscript in preparation.

percentage of heat-induced TA release from thermosensitive liposomes, based on which liposomal TA dosages were interpolated for each formulation to the in vivo situation.

2. MATERIALS AND METHODS

2.1 Materials

DPPC and MPPC were obtained from Avanti Polar Lipids (Alabaster, AL). DSPE-PEG (average PEG molecular mass of 2,000 amu), fluorescamine (4-phenylspiro-[furan-2(3H),1-phtha-

lan]-3,3′-dione), and HEPES (4-(2-hydroxyethyl)-1-piperazineethanesulfonic acid) sodium salt were acquired from Sigma Aldrich (St. Louis, MO). TA (4-(aminomethyl)cyclohexane-1-carboxylic acid) was purchased from Fluka (Buchs, Switzerland). All other chemicals used were analytical grade.

All concentrations listed throughout this manuscript refer to final concentrations unless indicated otherwise.

2.2 Liposome preparation and characterization

Large unilamellar vesicles prepared by extrusion technique (LUVETs) were prepared in the following compositions: DPPC, DPPC:DSPE-PEG (98:2, 96:4, and 94:6 molar ratios), DPPC:MPPC (90:10), and DPPC:MPPC:DSPE-PEG2000 (84:10:6 and 86:10:4). Phospholipids were dissolved in chloroform and mixed at the desired ratios. The solution was desiccated by evaporation under a stream of N_2 gas and exsiccated for 20 min in a vacuum exsiccator at room temperature (RT). The resulting lipid film was hydrated with 318 mM TA in 10 mM HEPES buffer (pH = 7.4, osmolarity = 0.302 osmol·kg^{-1}) (Osmomat 030 cryoscopic osmometer, Gonotec, Berlin, Germany) to a lipid concentration of 5 mM and bath sonicated for 10 min. The mixture was subjected to 10 freeze-thaw cycles and extruded 5 times through 0.2-μm Anopore aluminum oxide filters (Anotop, Whatman, Brentford, UK) at 55°C. The formulations were stored in the dark at 4°C until further use.

Unencapsulated TA was removed from the LUVET suspensions by size exclusion chromatography during 4-min centrifugation at 100 ×g and 4°C in a 2-mL syringe, containing a gel volume of 2.2-2.5 mL (Sephadex G-50 fine, GE Healthcare, Chalfont St. Giles, UK), and using a loading volume of 200 μL. The equilibration buffer, and thus the storage buffer for the LUVETs, consisted of 10 mM HEPES, 0.88% (w/v) NaCl, pH = 7.4, with an osmolarity of 0.291 osmol·kg^{-1}. As an internal control for the gel filtration efficiency, 200 mL of 318 mM TA in 10 mM HEPES buffer (pH = 7.4, osmolarity = 0.302 osmol·kg^{-1}) was loaded onto Sephadex G50 columns (n = 2 per experiment) and the eluent was assayed for TA content as described below. The mean±SD TA concentration in the eluent of control columns was 7.5±0.1% of the loaded liposomal TA concentration (n = 30).

For the heat-induced TA release experiments (section 2.5), the eluent from the first chromatography step was subjected to a second size exclusion chromatography step to ensure complete removal of unencapsulated TA.

Phospholipid concentrations were determined by the phosphorous assay according to Rouser et al. [18], and encapsulated TA was quantitated spectrofluorometrically as described in the next section. LUVET size and polydispersity were measured by photon correlation spectroscopy (PCS) at a 90° angle using unimodal analysis (Zetasizer 3000, Malvern Instruments, Malvern, UK) after dilution with equilibration buffer. LUVET phase transition temperatures were measured by differential scanning calorimetry (DSC, MicroCal, Northampton, MA) after dilution of LUVETs with equilibration buffer to a 3 mM final lipid concentration. Equilibration buffer was used as reference.

2.3 Spectrofluorometric quantification of tranexamic acid

For the spectrofluorometric determination of liposomal TA concentration, the LUVETs were

gel filtered as described in the previous section and diluted 500× with equilibration buffer. 500 µL of the LUVET solution was mixed with 250 µL of 5% TX100 (1% final concentration) and 500 µL of 1.08 mM fluorescamine in acetone (432 µM final concentration) [19]. Following 30 min incubation at 37°C, the samples were assayed spectrofluorometrically at λ_{ex} = 391±5 nm and λ_{em} = 483±5 nm (SPF 500C, American Instrument Company, Silver Springs, MD). Reference standards in the 0-4 µM TA concentration range were included in each separate experiment. Liposomal TA concentrations were derived by solving the regression equation of the reference curve for the respective fluorescence emission intensities. This protocol was used throughout the remainder of the work to determine TA:lipid ratios and to quantify heat-induced TA release.

The spectroscopic analysis of fluorescamine-derivatized TA as well as the effect of TX100 on the derivatization reaction are described in the appendix.

2.4 Calculation drug:lipid ratio, encapsulation efficiency, trapped volume, and endovesicular tranexamic acid concentration

Drug:lipid ratios were calculated by dividing the TA concentration as determined by the fluorescamine assay (corrected for the gel filtration efficiency) by the phospholipid concentration as determined by the Rouser assay.

The encapsulation efficiency, E_{eff}, was computed by dividing the liposomal TA:lipid molar ratio by the initial TA:lipid molar ratio (318 mM TA per 5 mM phospholipid, i.e., 63.6) and expressed as a percentage.

The trapped volume (V_t, L·mole^{-1} lipid) was computed with the equation (Eq.) obtained from [20]:

$$V_t = (500/3)(A)(N)(r_v) \quad \text{(Eq. 1)}$$

where A is the area of the membrane occupied by one lipid, N is the Avogadro constant (6.022×10^{23} mol^{-1}), and r_v the radius of the vesicle (based on PCS). The areas per phospholipid molecule were obtained from literature: 49.4 Å^2 for DPPC [21], 50.0 Å^2 for DSPE-PEG [22], and 48.0 Å^2 for MPPC [23]. For phospholipid mixtures, the areas were weighed averages indexed for the molar ratio of each lipid component:

$$A_{weighed} = [(A_{DPPC})(mol\%_{DPPC})+(A_{DSPE\text{-}PEG})(mol\%_{DSPE\text{-}PEG})+(A_{MPPC})(mol\%_{MPPC})]/100\% \quad \text{(Eq. 2)}$$

The $A_{weighed}$ was 49.4 Å^2 for all MPPC-lacking formulations and 49.3 Å^2 for the MPPC-containing formulations.

The V_t per vesicle (eV_t, expressed in L/vesicle) was derived by extrapolating the quantity of phospholipid molecules per vesicle. The quantity of phospholipid molecules per vesicle was defined as the cumulative number of lipids in the outer (l_{om}) and inner membrane leaflet (l_{im}), based on the $A_{weighed}$, the measured vesicle size with radius r_v, a bilayer thickness of 3.93 nm [24], and a spherical morphology (where area sphere = $4\pi r^2$):

$$I_{om} = 4\pi r_v^2/A_{weighed} \quad \text{(Eq. 3)}$$

$$I_{im} = 4\pi(r_v\text{-}3.93)^2/A_{weighed} \quad \text{(Eq. 4)}$$

The eV_t was calculated by:

$$eV_t = [(I_{om}+I_{im})V_t]/N \quad \text{(Eq. 5)}$$

The quantity of TA molecules per vesicle (Q_{TA}) was obtained by multiplying ($I_{om}+I_{im}$) by the TA:lipid ratio. Subsequently, the endovesicular TA concentration (C_{TA}) was computed from the amount of TA molecules per vesicle for a given eV_t:

$$C_{TA} = (Q_{TA}/N)(1/eV_t) \quad \text{(Eq. 6)}$$

2.5 Heat-induced tranexamic acid release

Active drug release from TA-encapsulating DPPC:DSPE-PEG (96:4) and DPPC:MPPC:DSPE-PEG (86:10:4) LUVETs was quantified following heat exposure near the maximum T_m and 4°C below the T_m by a method modified from [14].

Prior to heat treatment the gel filtered LUVET suspensions were diluted 10× with equilibration buffer that had been kept at 4°C. 20 µL of the gel filtered LUVET suspension was diluted 50-fold (n = 3 per experiment) and assayed spectrofluorometrically for total vesicular TA concentration (final dilution factor of 1250). The mean total vesicular TA concentration was used to calculate the percentage of released TA molecules.

Following 5 min equilibration at 4°C, 160 µL of the LUVETs was suspended in 0.2 mL ultra-thin PCR tubes (Thermowell Gold, Corning, New York, NY) and incubated at 4°C for 10 min before thermally-induced drug release, which was carried out in a thermal cycler (Biozym, Oldendorf, Germany). Samples were heated for a predefined period, after which they were immediately submersed in an ice bath. The entire volume was then transferred to 0.5 mL polycarbonate ultracentrifuge tubes and centrifuged (Optima TLX Ultracentrifuge, Beckman-Coulter, Fullerton, CA) at 355,000 ×g for 60 min at 4°C to pellet the LUVETs. 50 µL of the supernatant was carefully aspirated and the released TA in the supernatant was quantitated spectrofluorometrically following 50-fold dilution with equilibration buffer (final dilution factor of 1250). Phospholipid analysis of the supernatant showed that at least 99.9% of the phospholipids was pelleted. Four untreated 160-µL LUVET samples were included in the ultracentrifugation step to serve as negative control. These samples were processed in the same manner as the heat-treated samples to determine ultracentrifugation-induced TA leakage.

TA release was calculated by dividing the mean TA concentration in the supernatant of heat-treated samples by the mean total TA concentration in the LUVETs. TA concentrations were corrected for the mean TA content in the supernatant of the ultracentrifugation control samples. The mean±SD TA concentration in the supernatant of the centrifuge control samples of DPPC:DSPE-PEG (96:4) and DPPC:MPPC:DSPE-PEG (86:10:4) LUVETs was

2.4±5.1% (n = 48) and 7.1±11.1% (n = 56) of the total vesicular TA concentration, respectively.

2.6 Interpolation of liposomal tranexamic acid posology for the in vivo situation

In anticipation of in vivo proof-of-concept studies with the TA-encapsulating LUVETs, the minimum number of LUVETs and corresponding lipid concentrations that are required for a systemic TA concentration of 1.9 mM were computed for a 500-µm long vessel segment of port wine stain-typical diameters (30-200 µm [25]). The following assumptions were incorporated into the model calculations: approximately 7% of an individual's body weight (BW) is attributable to blood; blood has a specific gravity of 1.060 $kg \cdot L^{-1}$ (vs. 1.000 $kg \cdot L^{-1}$ for water); 55% of whole blood volume is plasma volume, of which 92% is water volume; and the target TA concentration ([TA]) is 10 $mg \cdot kg^{-1}$ body weight [26], corresponding to a final concentration of 1.9 mM. The number of minimally required LUVETs (L_m) for a vessel segment of length l and radius r, a given percentage of TA release (R_{TA}), and the quantity of TA molecules per vesicle (Q_{TA}) can subsequently be derived by the following equation:

$$L_m = (\pi r^2 l)[TA](N)(R_{TA})/Q_{TA} \quad \text{(Eq. 7)}$$

where the corresponding lipid concentration (C_{lip}) is calculated on the basis of the number of lipids in the outer and inner membrane ($l_{om}+l_{im}$) of a vesicle:

$$C_{lip} = (L_m(l_{om}+l_{im})/N)/(\pi r^2 l) \quad \text{(Eq. 8)}$$

Since L_m and C_{lip} can be calculated for a given blood volume ($\pi r^2 l$), the approximations can be extended to actual port wine stains if the total amount of blood per dermal volume is known. Consequently, the dermal blood volume of a typical port wine stain was calculated on the basis of a 3D histological reconstruction of a port wine stain biopsy [27], from which the number of minimally required LUVETs for a port wine stain, L_{PWS}, was subsequently derived as a function of port wine stain surface area. The histological reconstruction and related calculations are described in detail in the appendix.

2.7 Statistical analysis

Statistical analysis (means, standard deviations, linear regression analysis, Pearson's correlation analysis, and independent two-tailed homo- and heteroscedastic Student's t-tests) were performed with Statistical Package for Social Sciences (SSPS, Chicago, IL). The type of t-test used was predicated on Levene's test of equal variances. A p-value of ≤ 0.05, designated by (*), was considered statistically significant. A p-value of ≤ 0.01 is designated by (**) and not significant results by "N.S."

3. RESULTS

3.1 Spectrofluorometric quantification of fluorescamine-derivatized tranexamic acid

An assay based on primary amine derivatization with fluorescamine was developed for the quantification of liposomal TA in detergent-treated buffered solutions. Fluorescamine, which is non-fluorescent in native state, reacts readily and rapidly ($t_{1/2}$ = 0.1-0.5 s) with primary amines in a 1:1 stoichiometric ratio to yield highly fluorescent moieties (Fig. 2A) that can be quantified in the picomolar range. Non-reacted fluorescamine is hydrolyzed ($t_{1/2}$ = 5-10 s) to form non-fluorescent reaction products [19].

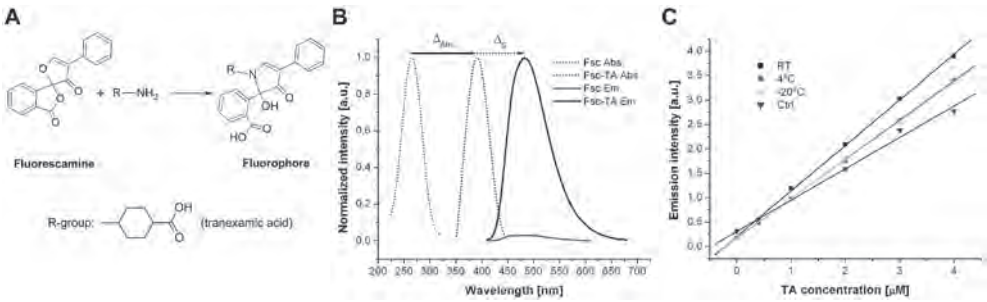

Figure 2. A) Fluorescamine reacts with compounds containing a primary amino group, such as tranexamic acid, to form fluorescent pyrrolinone-type moieties. Unreacted fluorescamine is hydrolyzed to form non-fluorescent reaction products. **B**) Normalized (to maximum) absorbance and emission spectra of unreacted fluorescamine (Fsc Abs and Fsc Em, respectively) and fluorescamine reacted with tranexamic acid (Fsc-TA Abs and Fsc-TA Em, respectively). The relative intensities between Fsc Em and Fcs-TA Em were maintained to show the lack of fluorescence of the former. **C**) Tranexamic acid (TA) was derivatized with fluorescamine in the presence of 1% Triton-X 100 and incubated for 30 min at RT (Ctrl) or for 24 h at RT, 4°C, or -20°C. The emission intensity [arbitrary units] is plotted vs. TA concentration within the TA calibration range as used in all experiments.

The formation of the fluorophore in the presence of TA was determined spectroscopically inasmuch as changes in chromophore structure are often associated with alterations in absorption and fluorescence properties. As shown in Fig. 2B, a shift in the absorption maximum (Δ_{Abs}) from 265 nm (non-reacted fluorescamine) to 391 nm (TA-reacted fluorescamine) and the appearance of a fluorescence emission peak (Δ_S) at 483 nm for the TA-fluorescamine reaction products corroborated the formation of the fluorophore.

Addition of 1% TX100 to the TA-fluorescamine reaction mixture slightly increased the amplitude of the fluorescence emission curve (λ_{range} = 415-675 nm) but did not affect the peak position (λ = 483 nm) or the linearity of the TA concentration-fluorescence emission intensity relationship (not shown). Incubation of TA and fluorescamine with TX100 for 24 h at RT, 4°C, and -20°C slightly affected the slope of the curve but not the linearity (Fig. 2C). Moreover, 24-h incubation at any temperature yielded higher fluorescence emission intensities relative to 30 min incubation, indicating that the reaction products remain stable for at least one day regardless of storage temperature. Although 24-h incubation at RT constituted the optimal reaction condition as evidenced by the relatively steep slope coefficient, linear regression analysis evinced that the other reaction conditions are equally suitable for the determination of TA concentration in detergent-treated buffered solutions ($R^2 > 0.9926$).

3.2 Drug:lipid ratios, vesicle sizes, and polydispersities

TA was encapsulated in LUVETs composed of DPPC (control), DPPC with increasing concentrations DSPE-PEG (2, 4, and 6 mol%), DPPC containing 10 mol% MPPC, and DPPC containing 6 mol% DSPE-PEG and 10 mol% MPPC. MPPC was incorporated into conventional thermosensitive formulations due to its ability to speed up release kinetics during phase transition [28]. The formulations were assayed for TA:lipid ratio, vesicle size, and the extent of size homogeneity (polydispersity).

The post-gel filtration TA:lipid ratios were 0.53-1.40% of the pre-gel filtration TA:lipid ratios, which is ascribable to the reduced TA-containing volume in the eluent (namely in the LUVETs only). Drug:lipid ratios can be used to deduce other outcome parameters (e.g., C_{TA}, L_m, and C_{lip}) in addition to providing insightful information when multiple formulations prepared in the same manner are juxtaposed. Notwithstanding the finding that the addition of PEG-conjugated DSPE at 2 and 4 mol% raised the TA:lipid ratio to respectively 0.89 (**) and 0.82 (*) vs. control (TA:lipid ratio of 0.63), increasing concentrations of DSPE-PEG imposed a deleterious effect on the mean TA:lipid ratio (Fig. 3A, formulations 2-4). DSPE-PEG concentrations of 6 mol% reduced the mean TA:lipid ratio by 16% (*) (Fig. 3A, formulation 4 vs. 1).

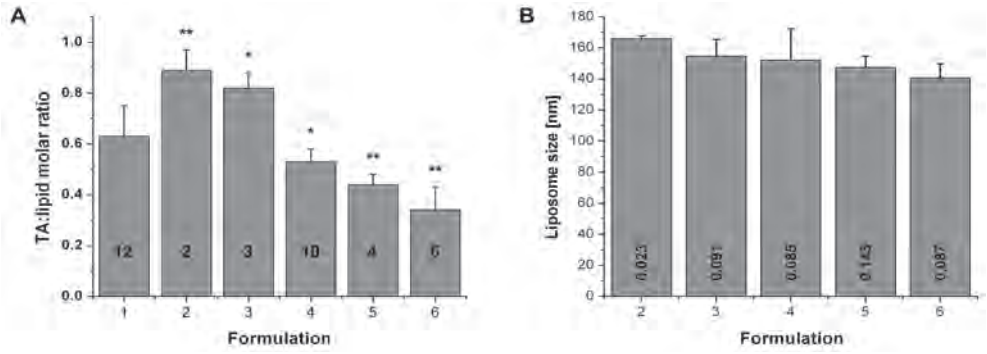

Figure 3. Tranexamic acid (TA):lipid ratios (**A**) and LUVET sizes (**B**) plotted for the six formulations assayed: 1: DPPC; 2: DPPC:DSPE-PEG (98:2 molar ratio); 3: DPPC:DSPE-PEG (96:4); 4: DPPC:DSPE-PEG (94:6); 5: DPPC:MPPC (90:10); and 6: DPPC:MPPC:DSPE-PEG2000 (84:10:6). Drug:lipid ratios were calculated by dividing the TA concentration as determined by the fluorescamine assay by the phospholipid concentration as determined by the Rouser assay as detailed in the experimental section. In (A) and (B), the numbers inside the bars indicate sample size and polydispersity index, respectively. Values were plotted as mean±SD. In (A), the level of significance is indicated vs. control.

Similarly, incorporation of 10 mol% MPPC into unPEGylated DPPC LUVETs exhibited a mean decrease of 30% (*) (Fig. 3A, formulation 5 vs. 1), whereas for DPPC:MPPC LUVETs containing 6 mol% DSPE-PEG (Fig. 3A, formulation 6) the reduction was 46% (**) relative to control.

Another relevant parameter is LUVET size, which should remain within a specific range (~0.16-0.21 μm) for effective evasion of the reticuloendothelial system (RES) during systemic circulation [29]. Liposomal formulations should therefore possess physicochemical properties that preclude aggregation/fusion. PCS revealed the sterically stabilizing effect of PEG, insofar as PEGylation deterred LUVET fusion and/or aggregation in buffer during storage.

The mean±SD vesicle size of extruded unPEGylated DPPC formulations was 1052±180 nm (> 5× greater than the filter pore size) with a mean polydispersity of 1.000 (result not shown), an effect that is consistent with previous reports [30]. Changes in polydispersity occurred within a few hours of storage at 4°C. In contrast, the mean sizes of the PEGylated LUVETs (Fig. 3B, formulations 2-4), which did not differ statistically from each other ($p \geq 0.212$), fell in the range of 152 to 166 nm with polydispersities of < 0.091. MPPC-containing formulations (Fig. 3B, formulations 5, 6) exhibited similar values. Interestingly, aggregation/fusion did not occur when MPPC was incorporated into unPEGylated DPPC LUVETs (Fig. 3B, formulation 5).

The results corroborate the importance of PEGylation but concomitantly underscore the balance that has to be struck between the level of "stealth" imposed on the formulation and endovesicular drug concentration, since these are apparently governed by an inversely proportional relationship. The incorporation of MPPC further undermined this balance. Accordingly, DPPC:DSPE-PEG (96:4) is the most suitable formulation for antifibrinolytic SSPLT based on the combination of TA:lipid ratio, size, and degree of steric stabilization [31].

3.3 Encapsulation efficiencies (E_{eff}), trapped volumes (V_t), and endovesicular TA concentrations (C_{TA})

Table 1 presents the E_{eff}, V_t, and C_{TA} of the formulations based on the experimentally obtained TA:lipid ratios and vesicle sizes, phospholipid molecular areas derived from literature, and the computed values summarized in Table 1 of the appendix. Since these outcome parameters are predominantly dependent on the former, the trends in E_{eff}, V_t, and C_{TA} conform to the trends exhibited by the TA:lipid ratios and LUVET sizes (Fig. 3).

The E_{eff} is a derivative of the drug:lipid ratio and is useful for relative interpretations as indicated above. A strong negative correlation existed between the E_{eff} and extent of PEGylation (Pearson's r = -0.915**), which, in relation to a uniform LUVET size distribution across the MPPC-lacking PEGylated formulations and the absence of a correlation between E_{eff} and size (r = -0.244, N.S.), implies a volumetric occupation by the PEG chains in the LUVET aqueous compartment (Table 1, formulations 2-4). The inclusion of MPPC further deteriorated the E_{eff} and caused a greater reduction in this parameter in conjunction with 6 mol% DSPE-PEG (Table 1, formulations 5 and 6, respectively, vs. 1, corresponding to reductions in E_{eff} of 29% and 46%, respectively).

	Formulation (mol%)	E_{eff}	V_t [L·mol^{-1}]	C_{TA} [M]
1	DPPC	0.98%	26.09	0.024
2	DPPC:DSPE-PEG2000 (98:2)	1.40%	4.11	0.217
3	DPPC:DSPE-PEG2000 (96:4)	1.29%	3.84	0.214
4	DPPC:DSPE-PEG2000 (94:6)	0.83%	3.78	0.140
5	DPPC:MPPC (90:10)	0.70%	3.72	0.119
6	DPPC:MPPC:DSPE-PEG2000 (84:10:6)	0.53%	3.56	0.095

Table 1. The encapsulation efficiency, E_{eff}, trapped volume, V_t, and endovesicular tranexamic acid (TA) concentration, C_{TA}, of the assayed formulations.

The V_ts were determined numerically based on the particle size data obtained by PCS, assuming a spherical morphology. The V_ts of the formulations (Table 1) fell in the range as reported in literature for comparable formulations [20,32], notwithstanding differences in

DPPC areas (A) [21] and the potential 20-40% volume overestimation as a result of morphology-related assumptions [32].

The C_{TA}, calculated on the basis of particle size, phospholipid area, and TA:lipid ratio, is a crucial parameter in relation to active release rates and targeting efficacy for it ultimately determines the clinical dosage. The C_{TA} should be maximized within physiological confines such as osmolarity and toxicity so that an optimal (local) drug concentration can be achieved with a minimal amount of vehicle. All formulations exhibited a reduced C_{TA} that comprised 68%-30% of the initial 318 mM TA concentration in the hydration solution. This was likely a result of the spatial occupation by PEG and, to a limited extent, of possibly aberrant phospholipid areas used in the computations. Nevertheless, conclusions can be drawn from the relative differences inasmuch as these are, in this case, hardly impacted by aberrant model assumptions. Formulations 4-6 had a significantly (**) reduced C_{TA} compared to formulations 2 and 3 (Table 1), implying that PEG concentrations >4 mol% and MPPC exerted a profound debilitating effect on the C_{TA}.

Taken altogether, DPPC:DSPE-PEG (96:4) remains the most suitable formulation for antifibrinolytic SSPLT given the negligible differences in E_{eff}, V_t, and C_{TA} between formulations 2 and 3.

3.4 Heat-induced drug release

Liposomes composed of phospholipids that have a T_m slightly above body temperature constitute ideal drug carriers for tissue targets that are easily accessible to artificially-induced hyperthermic conditions. Consequently, therapeutic agents loaded into thermosensitive liposomes can be actively released in a controlled fashion by heating the target site to T_m, which results in thermotropic alterations of the lipid bilayer and corollary increase in bilayer permeability and outward diffusion of encapsulated drugs [15]. To validate the hyperthermia model for two types of TA-encapsulating thermosensitive stealth formulations, TA-encapsulating DPPC:DSPE-PEG (96:4, T_m = 42.3°C, Fig. 4A) and DPPC:MPPC:DSPE-PEG (86:4:10, T_m = 41.5°C, Fig. 4B) LUVETs were heated from 4°C to 43.3°C and 40.0°C, respectively, and assayed for the percentage of TA release as a function of time.

The heating of DPPC/DSPE-PEG (96:4) LUVETs to phase transition caused a rapid release of TA that proceeded in a sigmoidal pattern (Fig. 4C). The most substantial release occurred between 0.5 and 2.5 min, corresponding to a mean release of 2.4% and 95.5%, respectively, and a mean release rate of 0.78%·s^{-1}. Moreover, TA release occurred at a very high release capacity (the maximum amount of drug released), approximating 100% within 2.5 min. Elevation of the temperature to 39.3°C (control) also induced drug release, but at a much slower rate, accounting for a release of ~13% after 5 min (Fig. 4C). This may have been due to the broader left transition shoulder as seen in the DPPC:DSPE-PEG thermogram (Fig. 4A), which entails the control temperature. The incorporation of 10 mol% MPPC sped up the release kinetics, whereby the most rapid drug release occurred between 0.5 (2.1%) and 2.0 min (93.0%), corresponding to a mean release rate of 1.02%·s^{-1} (Fig. 4D). Heating the formulation to 36.0°C resulted in negligible diffusion of TA from the LUVETs.

In light of the fast release kinetics and the high release capacity of the conventional thermosensitive formulation and the substantially reduced E_{eff} and C_{TA} of MPPC-containing

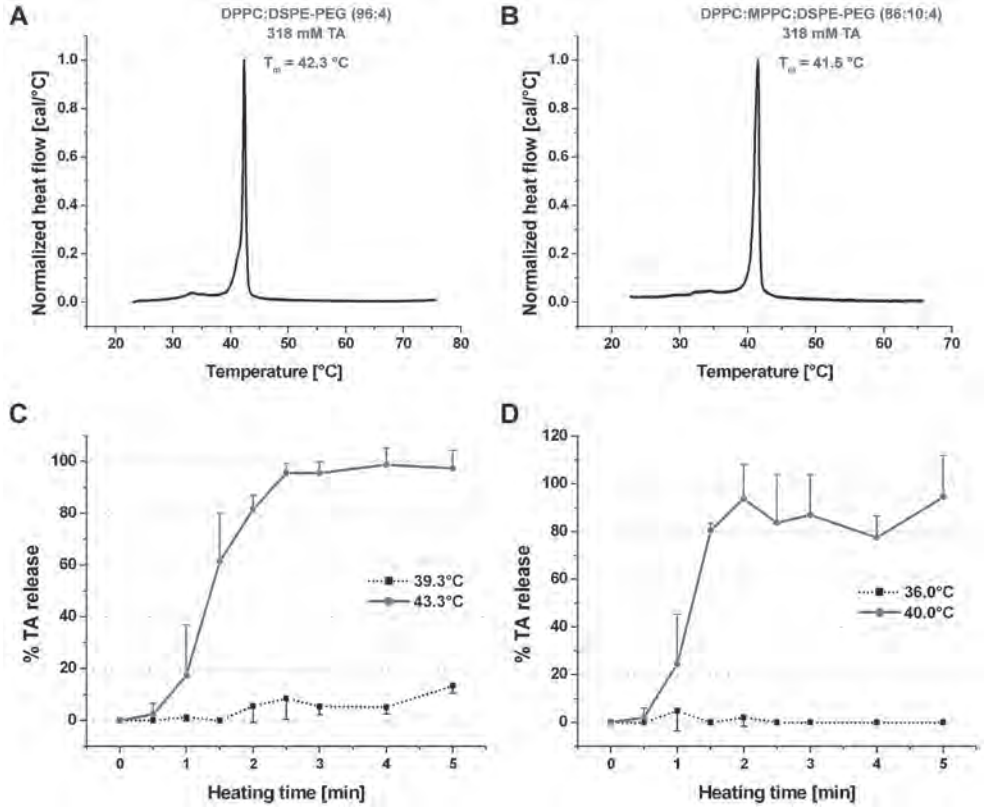

Figure 4. DSC thermograms of TA-encapsulating DPPC:DSPE-PEG (96:4) (**A**) and DPPC:MPPC:DSPE-PEG (86:10:4) (**B**) LUVETs. The phase transition temperature (T_m) is indicated next to the peak. (**C**) Heat-induced TA release from DPPC:DSPE-PEG (96:4) LUVETs plotted vs. heating time at 39.3°C (black, dotted line) and 43.3°C (gray, solid line). (**D**) Heat-induced TA release from DPPC:MPPC:DSPE-PEG (86:10:4) LUVETs plotted vs. heating time at 36.0°C (black, dotted line) and 40.0°C (gray, solid line). Released TA concentration is expressed as a mean±SD percentage of total liposomal TA concentration (n = 3 per time point).

LUVETs, the incorporation of MPPC yielded no surpassing advantages to advocate its potential applicability in the antifibrinolytic component of SSPLT.

3.5 Interpolated in vivo posologies

Following characterization of the LUVETs and determination of heat-induced drug release profiles, a model was developed to interpolate the number of TA-encapsulating LUVETs and final lipid concentrations required for an optimal antifibrinolytic effect in 500-µm long vessel segments of diameters that are representative for port wine stain vasculature. Final TA concentrations were predicated on clinically prescribed dosages, producing L_m (number of minimally required LUVETs) ranges in the order of 10^6-10^8 for 30-200-µm vessel diameters, respectively (Fig. 5A, B). The C_{lip} (lipid concentration) values comprised 2.1, 2.7, and 4.3 mM for DPPC:DSPE-PEG LUVETs with 98:2, 96:4, and 94:6 molar ratios, respectively, and 5.6 and 8.0 mM for DPPC:MPPC (90:10) and DPPC:MPPC:DSPE-PEG (84:10:6) LUVETs, respectively.

Computational analysis was subsequently performed on a 3D histological reconstruction of a port wine stain (Fig. 5C) to derive the dermal blood volume, which yielded 2.15 µL blood per cm^2 skin surface (appendix). With a target TA concentration of 1.9 mM and an approximated quantity of TA molecules per vesicle (Q_{TA}) for each formulation (appendix), the L_{PWS} could be interpolated for port wine stains of different surface areas (A_{PWS}) as presented in Fig. 5C. For A_{PWS} between 5 and 40 cm^2, the L_{PWS} ranged from 41-327 for DPPC:DSPE-PEG (98:2) at the lower end and from 156-1247 for DPPC:MPPC:DSPE-PEG2000 (84:10:6) at the upper end, respectively.

4. DISCUSSION

Selective photothermolysis, or the selective destruction of blood vessels by pulsed laser irradiation, was introduced in the early 80's as a means to non-invasively remove aberrant cutaneous vasculature through controllable photothermal processes [33]. Presently, selective photothermolysis represents the gold standard for the treatment of port wine stains (capillary malformations), with extended applicability in dermatology and ophthalmology [34]. Although port wine stains can be effectively treated by selective photothermolysis, there are several inevitable intrinsic factors, including epidermal pigmentation [35], optical shielding by blood and superimposed vessels [36-38], and port wine stain anatomy and morphology [8,39,40], that are responsible for suboptimal outcomes in approximately 60% of patients [37,41]. Inasmuch as these factors are difficult to circumvent completely by external means (e.g., by using different laser parameters [39-41] or dynamic cooling [42]), SSPLT was devised to

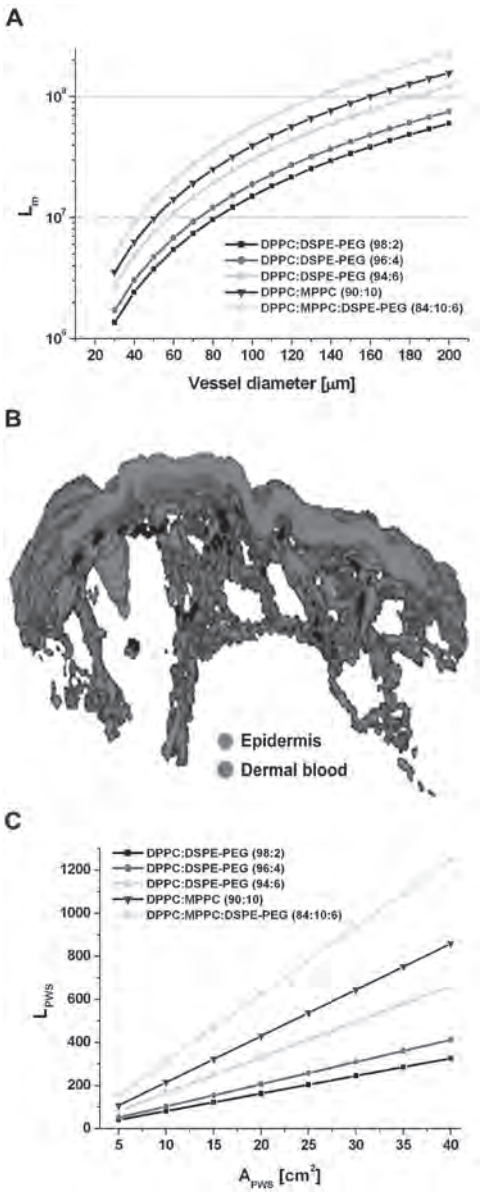

Figure 5. The number of LUVETs (L_m) (**A**) minimally required to achieve a TA concentration of 1.9 mM in a 500-µm long vessel segment, plotted as a function of vessel diameter. **B**) 3D histological reconstruction of a port wine stain biopsy, from which the number of minimally required LUVETs for a port wine stain (L_{PWS}) was derived as a function of port wine stain surface area (**C**).

tackle poor lesional clearance rates from within the vasculature.

As presented in the legend of Fig. 1, SSPLT entails a prothrombotic component and an antifibrinolytic component. In an effort to develop an antifibrinolytic drug delivery platform for SSPLT, a liposomal system was selected for the encapsulation of TA, a potent antifibrinolytic agent used in the clinical setting to inhibit plasmin-mediated thrombolysis. Inasmuch as SSPLT relies on the laser-induced generation of heat, the rudimentary design of liposomes was based on thermosensitivity as the main drug release mechanism. Hence, TA-encapsulating DPPC(:MPPC) and DPPC(:MPPC):DSPE-PEG formulations were assayed for TA:lipid ratio and size so as to derive E_{eff}, V_t, and C_{TA}, after which heat-induced TA release was quantified for the most optimal candidate formulation in the absence and presence of lysolipid. In the final analysis, LUVETs composed of DPPC:DSPE-PEG in a 96:4 molar ratio came out as the prime formulation for antifibrinolytic SSPLT.

The most relevant parameters regarding DPPC:DSPE-PEG (96:4) LUVETs in light of the further development of SSPLT as a clinical modality include the TA:lipid ratio, E_{eff}, C_{TA} and the release kinetics, inasmuch as these chiefly dictate posology. At a mean TA:lipid ratio of 0.82 and an E_{eff} of 1.29%, the prime candidate formulation encompassed a C_{TA} of 214 mM and a release rate of approximately 100% in 2.5 min. Notwithstanding differences in liposome composition, the TA:lipid ratio of DPPC:DSPE-PEG LUVETs was comparable to or higher than drug:lipid ratios reported for liposome-encapsulated anti-cancer drugs such as doxorubicin, paclitaxel, N3-O-toluyl-5-fluorouracyl, and ZD6126 (Table 3, appendix). In contrast, the encapsulation efficiency was substantially lower than most of the compounds reviewed (Table 3, appendix), which is likely the result of the relatively high initial TA:lipid ratio (63.6) and the excessive removal of unencapsulated TA during size-exclusion chromatography in combination with the preparation technique (hydration of lipid film).

A rather unexpected finding was that heat-induced TA release from the candidate formulation occurred at an exceptionally fast rate and at a ~100% release capacity. David Needham's group reported release times and release capacities in the order of ~5 min and ~85% release of carboxyfluorescein from lysolecithin (MPPC)-containing thermosensitive liposomes, respectively, ~20 min and ~40% release of doxorubicin from traditional thermosensitive liposomes (comparable to our candidate formulation), respectively, and ~5 min and ~50% release of doxorubicin from MPPC-containing thermosensitive liposomes, respectively [15]. A marked contribution of MPPC to the release kinetics, as has been reported previously [15,28], remained absent with respect to TA-encapsulating DPPC:DSPE-PEG (96:4) LUVETs. Although the exact reasons for these substantial differences are presently unknown, the small size of TA may contribute to a less constrained passage through the laterally decompressed membrane during phase transition – a phenomenon that is accompanied by a greater membrane hydration state [43], corollary packing defects and cavitation [44], and a lowered transmembrane free energy barrier [45,46], all of which actuate a greater extent of diffusion of ions and supposedly higher molecular weight compounds such as doxorubicin and carboxyfluorescein vs. gel phase or liquid crystalline states. It is expected that, under these conditions, smaller molecules (e.g., TA) transgress the membrane more facilely than larger ones (e.g., carboxyfluorescein and doxorubicin).

The exact explication notwithstanding, the release kinetics of DPPC:DSPE-PEG (96:4)

LUVETs are, within the limits of the in vitro data, ideal in the context of selective photothermolysis-related endovascular laser-tissue interactions [1]. The hemodynamic response (thrombosis), that occurs in consequence to the photothermal response (laser-induced thermal coagulum formation), is characterized by a growth phase and a deterioration phase (manuscript in preparation). The hemostatic equilibrium shifts to a predominantly prothrombotic state during the growth phase and to a predominantly fibrinolytic state during the deterioration phase. Using a hamster dorsal skin fold model in combination with laser-mediated endovascular damage induction [3], we have demonstrated that the prothrombotic state reaches a maximum at approximately 6.25 min following laser irradiation ([4], manuscript in preparation). In order to extend this state through the inhibition of fibrinolysis, accumulation of the drug carrier is exacted during the early formative stages of the thrombus so that TA-encapsulating liposomes can progressively accumulate into the developing clot in concurrence with plasminogen [47] and, particularly in venules [48], its agonist tissue plasminogen activator (tPA) [13]. Theoretically, this should be possible given the rapid release kinetics of the DPPC:DSPE-PEG LUVETs compared to the 2.5-fold longer duration of the growth phase, allowing TA to first accumulate at the target site and then be released into the clot before (and during) the transition to a fibrinolytic state. Furthermore, the high release capacity of this formulation is considerably advantageous since about three LUVETs are required to completely inhibit plasminogen bound to one activated platelet, taking into account a saturation level of $1.9\pm0.5\times10^5$ plasminogen molecules per platelet [47], 5 lysine binding sites per plasminogen molecule [49], and the encapsulation of roughly 3×10^5 TA molecules per LUVET (appendix).

Secondly, the favorable release kinetics and release capacity of DPPC:DSPE-PEG LUVETs enforce the potential applicability of the envisaged SSPLT regime in a clinical setting. The therapeutic procedures may be performed on an outpatient basis, whereby the LUVET formulation would be systemically administered 10-15 min before laser treatment to ensure homogenous distribution throughout the circulation. Subsequently, a lasing regime would be performed on the port wine stain to induce the hemodynamic response, after which the irradiated region is selectively heated, e.g., by a heating pad or near infra-red light, to trigger drug release so as to facilitate complete emphraxis of the semi-coagulated vasculature. Since this has to occur within the time span of the hemodynamic response, the total duration of the actual procedure will be determined chiefly by the number of lasing/heating cycles needed to treat the entire port wine stain, which in turn depends on the size of the lesion. The majority of port wine stains is <40 cm^2 in size [50], which eliminates the need for excessively long treatment sessions.

In conclusion, several rudimentary liposomal formulations were explored for the antifibrinolytic component of SSPLT and their properties and heat-induced release profiles juxtaposed to selective photothermolysis-related endovascular laser-tissue interactions and criteria for clinical application. Although several features will have to be optimized and/or added (e.g., targeting), DPPC:DSPE-PEG (96:4) LUVETs evolved as the prime candidate formulation. In light of forthcoming in vivo research, models were developed to facilitate LUVET accumulation and release experiments in singular vessels such as in [2,3] or to further assess posology based on port wine stain dimensions. In case of the former, assays could be set up by using fluorescently-labeled LUVETs and correlating the emitted fluorescence from ac-

cumulated LUVETs in laser-induced thrombi to a lipid or LUVET concentration. Subsequently, heat-induced TA release from the accumulated LUVETs could be quantified from blood as described in [14]. The mathematical approximations and computational models presented here will also be useful in current and future research aimed at vehicular targeting, including thermosensitive immunoLUVETs that recognize specific epitopes on activated platelets or fibrin, and the prothrombotic component of SSPLT.

Acknowledgments

This work was in part supported by the Technological Collaboration Grant (TSGE 1048) of the Dutch Ministry of Economic Affairs (MH, JFB), NanoNed (IH, AIdK), the Arnold and Mabel Beckman Foundation (BC), and the U.S. National Institute of Health Laser Microbeam and Medical Program (BC). M.H. was partially supported by a personal grant from Novo Nordisk Farma BV. We thank Dr. Josh Pfeffer for constructive input on the 3D reconstruction analysis.

REFERENCES

1. M. Heger, J.F. Beek, N.I. Moldovan, C.M. van der Horst, M.J. van Gemert, Towards optimization of selective photothermolysis: prothrombotic pharmaceutical agents as potential adjuvants in laser treatment of port wine stains. A theoretical study, Thromb. Haemost. 93(2) (2005) 242-256.
2. M. Heger, J.F. Beek, K. Stenback, D.J. Faber, M.J. van Gemert, C. Ince, Darkfield orthogonal polarized spectral imaging for studying endovascular laser-tissue interactions in vivo – a preliminary study, Opt. Express 13(3) (2005) 702-715.
3. R. Bezemer, M. Heger, J.P. van den Wijngaard, S.R. Mordon, M.J. van Gemert, J.F. Beek, Laser-induced (endo)vascular photothermal effects studied by combined brightfield and fluorescence microscopy in hamster dorsal skin fold venules, Opt. Express 15(14) (2007) 8493-8506.
4. M. Heger, I.I. Salles, R. Bezemer, S. Mordon, S. Begu, N. Jouy, H. Deckmyn, M.J. van Gemert, J.F. Beek, Thrombosis as an integral part of endovascular laser-tissue interactions, Lasers Surg. Med. Suppl. 18(11) (2006) 5.
5. W. Verkruysse, G.W. Lucassen, M.J. van Gemert, Simulation of color of port wine stain skin and its dependence on skin variables, Lasers Surg. Med. 25(2) (1999) 131-139.
6. G.W. Lucassen, W. Verkruysse, M. Keijzer, M.J. van Gemert, Light distributions in a port wine stain model containing multiple cylindrical and curved blood vessels, Lasers Surg. Med. 18(4) (1996) 345-357.
7. E.J. Fiskerstrand, L.O. Svaasand, G. Kopstad, K. Ryggen, S. Aase, Photothermally induced vessel-wall necrosis after pulsed dye laser treatment: lack of response in port-wine stains with small sized or deeply located vessels, J. Invest. Dermatol. 107(5) (1996) 671-675.
8. E.J. Fiskerstrand, L.O. Svaasand, G. Kopstad, M. Dalaker, L.T. Norvang, G. Volden, Laser treatment of port wine stains: therapeutic outcome in relation to morphological parameters, Br. J. Dermatol. 134(6) (1996) 1039-1043.
9. J.H. Levy, Pharmacologic preservation of the hemostatic system during cardiac surgery, Ann. Thorac. Surg. 72(5) (2001) S1814-S1820.
10. J. Karski, G. Djaiani, J. Carroll, M. Iwanochko, P. Seneviratne, P. Liu, W. Kucharczyk, L. Fedorko, T. David, D. Cheng, Tranexamic acid and early saphenous vein graft patency in conventional coronary artery bypass graft surgery: a prospective randomized controlled clinical trial, J. Thorac. Cardiovasc. Surg. 130(2) (2005) 309-314.
11. P.M. Mannucci, Treatment of von Willebrand's disease, N. Engl. J. Med. 351(7) (2004) 683-694.
12. M. Hoylaerts, H.R. Lijnen, D. Collen, Studies on the mechanism of the antifibrinolytic action of tranexamic acid, Biochim. Biophys. Acta 673(1) (1981) 75-85.
13. L. Medved, W. Nieuwenhuizen, Molecular mechanisms of initiation of fibrinolysis by fibrin, Thromb. Haemost. 89(3) (2003) 409-419.
14. J.F. Huertas-Pérez, M. Heger, H. Dekker, H. Krabbe, J. Lankelma, F. Ariese, Simple, rapid, and sensitive liquid chromatography-fluorescence method for the quantification of tranexamic acid in blood, J. Chromatogr. A 1157(1-2) (2007) 142-150.
15. D. Needham, M.W. Dewhirst, The development and testing of a new temperature-sensitive drug delivery system for the treatment of solid tumors, Adv. Drug Deliv. Rev. 53(3) (2001) 285-305.
16. K. Maruyama, S. Unezaki, N. Takahashi, M. Iwatsuru, Enhanced delivery of doxorubicin to tumor by long-circulating thermosensitive liposomes and local hyperthermia, Biochim. Biophys. Acta 1149(2) (1993) 209-216.
17. M.H. Gaber, N.Z. Wu, K. Hong, S.K. Huang, M.W. Dewhirst, D. Papahadjopoulos, Thermosensitive liposomes: extravasation and release of content in tumor microvascular networks. Int. J. Radiat. Oncol. Biol. Phys. 36(5) (1996) 1177-1187.
18. G. Rouser, S. Fleischer, A. Yamamoto, Two-dimensional thin layer chromatographic separation of polar lipids and determination of phospholipids by phosphorous analysis of spots, Lipids 5(5) (1970) 494-496.
19. S. Udenfriend, S. Stein, P. Böhlen, W. Dairman, W. Leimgruber, M. Weigele, Fluorescamine: a reagent for assay of amino acids, peptides, proteins, and primary amines in the picomole range, Science 178(63) (1972) 871-872.
20. N.J. Zuidam, R. de Vrueh, D.J. Crommelin, in: V.P. Torchilin, V. Weissig (Eds.), Liposomes, 2nd Edition, Oxford University Press, Oxford, 2003, pp. 64.
21. J.F. Nagle, S. Tristam-Nagle, Lipid bilayer structure, Curr. Opin. Struc. Biol. 10(4) (2000) 474-480.
22. J. Majewski, T.L. Kuhl, K. Kjaer, M.C. Gerstenberg, J. Als-Nielsen, J.N. Isrealachvili, G.S. Smith, X-ray synchrotron study of packing and protrusions of polymer-lipid monolayers at the air-water interface, J. Am. Chem. Soc. 120(7) (1998) 1469-1473.
23. L.M. Chi, W.G. Wu, Effective bilayer expansion and erythrocyte shape change induced by monopalmitoyl phosphatidylcholine. Quantitative light microscopy and nuclear magnetic resonance spectroscopy measurements, Biophys. J. 57(6) (1990) 1225-1232.
24. Y. Tahara, Y. Fujiyoshi, A new method to measure bilayer thickness: cryo-electron microscopy of frozen hydrated liposomes and image simulation, Micron 25(2) (1994) 141-149.

25. M.M. Selim, K.M. Kelly, J.S. Nelson, G. Wendelschafer-Crabb, W.R. Kennedy, B.D. Zelickson, Confocal microscopy study of nerves and blood vessels in untreated and treated port wine stains: preliminary observations, Dermatol. Surg. 30(6) (2004) 892-897.
26. S. Chauhan, P. Gharde, A. Bisoi, S. Kale, U. Kiran, A comparison of aminocaproic acid and tranexamic acid in adult cardiac surgery, Ann. Card. Anaesth. 7(1) (2004) 40-43.
27. D.J. Smithies, M.J. van Gemert, M.K. Hansen, T.E. Milner, J.S. Nelson, Three-dimensional reconstruction of port wine stain vascular anatomy from serial histological sections, Phys. Med. Biol. 42(9) (1997) 1843-1847.
28. G.R. Anyarambhatla, D. Needham, Enhancement of the phase transition permeability of DPPC liposomes by incorporation of MPPC: a new temperature-sensitive liposome for use with mild hyperthermia, J. Liposome Res. 9(4) (1999) 491-506.
29. V.D. Awasthi, D. Garcia, B.A. Goins, W.T. Phillips, Circulation and biodistribution profiles of long-circulating PEG-liposomes of various sizes in rabbits, Int. J. Pharm. 253(1-2) (2003) 121-132.
30. S. Sriwongsitanont, M. Ueno, Effect of a PEG lipid (DSPE-PEG2000) and freeze-thawing process on phospholipid vesicle size and lamellarity, Colloid Polym. Sci. 282(7) (2004) 753-760.
31. C. Vermehren, K. Jørgensen, S. Frokjaer, Influence of lipopolymer concentration on liposome degradation and blood clearance, Int. J. Pharm. 183(1) (1999) 13-16.
32. D. Huster, A.J. Jin, K. Arnold, K. Gawrisch, Water permeability of polyunsaturated lipid membranes measured by 17O NMR, Biophys. J. 73(2) (1997) 855-864.
33. R.R. Anderson, J.A. Parrish, Selective photothermolysis: precise microsurgery by selective absorption of pulsed radiation, Science 220(4596) (1983) 524-527.
34. D.J. Leffell, J.T. Thompson, Lasers in dermatology and ophthalmology, Dermatol. Clin. 10(4) (1992) 687-700.
35. W. Verkruysse, G.W. Lucassen, M.J. van Gemert, Simulation of color of port wine stain skin and its dependence on skin variables, Lasers Surg. Med. 25(2) (1999) 131-139.
36. G.W. Lucassen, W. Verkruysse, M. Keijzer, M.J. van Gemert, Light distributions in a port wine stain model containing multiple cylindrical and curved blood vessels, Lasers Surg. Med. 18(4) (1996) 345-357.
37. U. Hohenleutner, M. Hilbert, U. Wlotzke, M. Landthaler, Epidermal damage and limited coagulation depth with the flashlamp-pumped pulsed dye laser: a histochemical study, J. Invest. Dermatol. 104(5) (1995) 798-802.
38. E.J. Fiskerstrand, L.O. Svaasand, G. Kopstad, K. Ryggen, S. Aase, Photothermally induced vessel-wall necrosis after pulsed dye laser treatment: lack of response in port-wine stains with small sized or deeply located vessels, J. Invest. Dermatol. 107(5) (1996) 671-675.
39. W. Verkruysse, J.W. Pickering, J.F. Beek, M. Keijzer, M.J. van Gemert, Modeling the effect of wavelength on the pulsed dye laser treatment of port wine stains, Appl. Optics 32(4) (1993) 393-398.
40. M.J. van Gemert, D.J. Smithies, W. Verkruysse, T.E. Milner, J.S. Nelson, Wavelengths for port wine stain laser treatment: influence of vessel radius and skin anatomy, Phys. Med. Biol. 42(1) (1997) 41-50.
41. B. Greve, C. Raulin, Prospective study of port wine stain treatment with dye laser: comparison of two wavelengths (585 nm vs. 595 nm) and two pulse durations (0.5 milliseconds vs. 20 milliseconds), Lasers Surg. Med. 34(2) (2004) 168-173.
42. K.M. Kelly, V.S. Nanda, J.S. Nelson, Treatment of port-wine stain birthmarks using the 1.5-msec pulsed dye laser at high fluences in conjunction with cryogen spray cooling, Dermatol. Surg. 28(4) (2002) 309-313.
43. D. Marsh, General features of phospholipid phase transitions, Chem. Phys. Lipids 57(2-3) (1991) 109-120.
44. E.A. Evans, R. Waugh, Mechano-chemistry of closed, vesicular membrane systems, J. Colloid Interface Sci. 60(2) (1977) 286-298.
45. J.F. Nagle, H.L. Scott, Lateral compressibility of lipid mono- and bilayers. Theory of membrane permeability, Biochim. Biophys. Acta 513(2) (1978) 236-243.
46. S. Doniach, Thermodynamic fluctuations in phospholipid bilayers, J. Chem. Phys. 68(11) (1978) 4912-4916.
47. L.A. Miles, E.F. Plow, Binding and activation of plasminogen on the platelet surface, J. Biol. Chem. 260(7) (1985) 4303-4311.
48. E.g., Levin, L. Santell, K.G. Osborn, The expression of endothelial tissue plasminogen activator in vivo: a function defined by vessel size and anatomic location, J. Cell Sci. 110(Pt 2) (1997) 139-148.
49. G. Markus, R.L. Priore, F.C. Wissler, The binding of tranexamic acid to native (Glu) and modified (Lys) human plasminogen and its effect on conformation, J. Biol. Chem. 254(4) (1979) 1211-1216.
50. C.M. Nguyen, J.J. Yohn, C. Huff, W.L. Weston, J.G. Morelli, Facial port wine stains in childhood: prediction of the rate of improvement as a function of the age of the patient, size and location of the port wine stain and the number of treatments with the pulsed dye (585 nm) laser, Br. J. Dermatol. 138(5) (1998) 821-825.

7

Tranexamic acid-containing thermosensitive liposomal formulations for antifibrinolytic site-specific pharmaco-laser therapy

Appendix

INDEX OF ABBREVIATIONS

A_{PWS}	- port wine stain surface area
C_{TA}	- endovesicular tranexamic acid concentration
DPPC	- 1,2-dipalmitoyl-*sn*-glycero-3-phosphatidylcholine
DSPE-PEG2000	- 1,2-distearoyl-*sn*-glycero-3-phosphatidylethanolamine-polyethylene glycol (PEG MW = 2000 g·mol^{-1})
eV_t	- trapped volume per vesicle
IM	- inner membrane
l	- vessel length
L_m	- number of minimally required LUVETs
L_{PWS}	- number of minimally required LUVETs for a port wine stain
LUVET	- large unilamellar vesicle prepared by extrusion technique
MPPC	- 1-palmitoyl-2-hydroxy-*sn*-glycero-3- phosphatidylcholine
MW	- molecular weight
OM	- outer membrane
Q_{TA}	- quantity of TA molecules per vesicle
r	- vessel radius
SSPLT	- site-specific pharmaco-laser therapy
TA	- tranexamic acid (4-(aminomethyl)cyclohexane-1-carboxylic acid)

METHODS AND RESULTS

The supplemental methods and results are presented in the order of the manuscript under the respective headings.

2.3 Spectrofluorometric quantification of tranexamic acid

To demonstrate the conversion of fluorescamine to its fluorophore state in the presence of TA, the absorption (Lambda 18, Perkin Elmer, Wellesley, MA) and fluorescence emission spectra (SPF 500C, American Instrument Company, Silver Springs, MD) were acquired of 7.95 mM TA in 9.96 mM HEPES reacted with 4.5 µM fluorescamine and 5 µM TA in 5 mM HEPES reacted with 504 µM fluorescamine, respectively. TA and HEPES stock solutions were adjusted to pH = 7.4 prior to mixing with stock aliquots of 1.08 mM fluorescamine in acetone [1]. Reaction mixtures were incubated for 30 min at 37°C during continuous shaking before spectroscopic analysis. Fluorescence emission spectra were acquired at λ_{ex} = 391±5 nm, i.e., the absorption maximum of TA-reacted fluorescamine (Fig. 2B, main manuscript).

Regression analysis was performed in order to assess the degree of linearity between TA concentration and fluorescence emission intensity in a predetermined titration range. 500 µL of the TA standard solution (0.0, 0.4, 1.0, 2.0, 3.0, 4.0 µM in 10 mM HEPES, pH = 7.4) was mixed with 250 µL of 10 mM HEPES, pH = 7.4 (2 mM final concentration) and 500 µL of 1.08 mM fluorescamine in acetone (432 µM final concentration) to a final volume of 1.25 mL. The samples were thermomixed in the dark for 30 min at 37°C. TA concentration was assayed spectrofluorometrically at λ_{ex} = 391±5 nm and λ_{em} = 483±5 nm. A linear fit yielded a mean R^2 of 0.996 in this concentration range (n=10).

To rule out any detrimental effects of TX100 on the linear relationship between TA concentration and fluorescence emission and to measure the stability of the fluorophore as a function of time and temperature, TA samples were prepared as above except for the addition of 250 µL of 5% (v/v) TX100 in water (1% final concentration) instead of 250 µL HEPES buffer. Spectrofluorometric measurements were performed immediately following 30 min incubation at 37°C and after 24-h storage at RT, 4°C, and -20°C (Fig. 2C, main manuscript).

2.4 Calculation drug:lipid ratio, encapsulation efficiency, trapped volume, and endovesicular tranexamic acid concentration

In order to calculate the C_{TA}, the number of TA molecules per LUVET and the eV_t had to be derived from the mean LUVET sizes, the phospholipid molecular areas, and the measured TA:lipid ratios. Table 1 lists the derived data that were used to calculate the C_{TA}.

	Formulation (mol%)	OM surface (nm^2)	IM surface (nm^2)	No. of lipids OM	No. of lipids IM	Lipids per vesicle	Q_{TA}	eV_t (L/vesicle)
1	DPPC	3,480,638	3,428,839	7,045,825	6,940,969	13,986,794	8,744,807	6.06×10^{-16}
2	DPPC:DSPE-PEG2000 (98:2)	86,500	78,498	175,059	158,864	333,923	298,165	2.28×10^{-18}
3	DPPC:DSPE-PEG2000 (96:4)	75,167	67,720	152,085	137,019	289,104	237,516	1.84×10^{-18}
4	DPPC:DSPE-PEG2000 (94:6)	72,804	65,478	147,269	132,451	279,720	147,848	1.75×10^{-18}
5	DPPC:MPPC (90:10)	68,315	61,225	135,923	121,817	257,740	114,195	1.59×10^{-18}
6	DPPC:MPPC:DSPE-PEG2000 (84:10:6)	62,474	55,703	124,213	110,750	234,963	79,027	1.39×10^{-18}

Table 1. List of parameters derived from experimental data that were used to calculate the C_{TA}.

2.6 Interpolation of liposomal tranexamic acid posology for the in vivo situation

The 3D reconstruction of the port wine stain biopsy from serial histological sections has been described in [2]. A 3-mm punch biopsy was obtained from a refractory port wine stain on the forearm. The tissue was embedded in paraffin, after which 6-µm thick sections were cut and stained with hematoxylin and eosin (H&E). The sections were imaged with a 640×480 color CCD video camera at a 20× magnification, whereby 3 overlapping 2D images were acquired and aligned to reconstruct the entire section in one composite image. Seventy consecutive sections were lined up to comprise the 3D image.

Interactive utilities were programmed for AVS image visualization software (Advanced Visual System, Waltham, MA) as described in [3]. The programmed utilities combined the images, outlined and stored the position of the epidermal region and vessel circumference, and reconstructed the 3D vasculature from the recorded position of the epidermis and vessels. The lines encompassing the epidermis and blood vessels for each composite 2D image were rotated and translated so that the corresponding regions of consecutive sections coincided. The 3D reconstruction was subsequently composed with standard linear algebra techniques.

The blood volume was derived from a 3D matrix of 358 (depth) × 772 (length) × 70 (number of sections) data points, corresponding to tissue dimensions of 0.716 mm × 1.544

mm × 0.420 mm, respectively. The total dermal volume was quantified from the bottom of the epidermal layer (determined for each column) to the bottom of the section. The blood volume was calculated per 2D section by counting the number of pixels required to fill the regions delineated by the entered vessel circumferences. The cumulative number of 'blood pixels' in the 70 sections hence represented the dermal blood volume.

A blood fraction of 3% was computed in the dermal volume, which comprised 79% of the entire skin specimen. The 3% dermal blood volume most likely represented a lower bound for this specific biopsy region inasmuch as a blood fraction of 4% was calculated when only columns 300-500 of the sections were analyzed. This discrepancy resulted from the fact that the histology section did not have well-defined lateral boundaries. Consequently, a 3.5% dermal blood volume was used in further calculations.

Based on the computational analysis, a typical port wine stain with a surface area of 0.65 mm^2 and a skin volume of 0.46 mm^3 has a dermal volume of 0.39 µL (85% of analyzed skin volume) and a corresponding dermal blood volume of 14 nL, which translates into 2.15 µL blood per cm^2 of skin surface. The number of minimally required LUVETs per µL of blood was then calculated by $L_m/(\pi r^2 l)$ after solving for L_m with predefined vessel segment dimensions (vessel with radius, *r*, and length, *l*) using Equation 7 (manuscript). The number of minimally required LUVETs per µL blood is presented for each candidate formulation in Table 2.

	Formulation (mol%)	$L_m \cdot \mu L^{-1}$
2	DPPC:DSPE-PEG2000 (98:2)	3.8
3	DPPC:DSPE-PEG2000 (96:4)	4.8
4	DPPC:DSPE-PEG2000 (94:6)	7.7
5	DPPC:MPPC (90:10)	10.0
6	DPPC:MPPC:DSPE-PEG2000 (84:10:6)	14.5

Table 2. The number of minimally required LUVETs (L_m) indicated per µL blood for every SSPLT candidate formulation. Values are predicated on 100% TA release from thermosensitive LUVETs.

The number of minimally required LUVETs for a port wine stain (L_{PWS}) was subsequently plotted as a function of port wine stain surface area (A_{PWS}) for every candidate formulation by solving for:

$$L_{PWS} = (L_m \cdot \mu L^{-1})(2.15\ \mu L \cdot cm^{-2})(A_{PWS}) \quad \text{(Eq. 2)}$$

where $(L_m \cdot \mu L^{-1})$ was based on the values in Table 2.

DISCUSSION

A comprehensive overview of drug:lipid ratios and encapsulation efficiencies of various liposomal compounds is presented in Table 3.

Ref.	Formulation (mole ratio)	Encapsulant	Drug:Lipid Ratio	E_{eff} [%]
[4]	DPPC:HSPC:chol:DSPE-PEG (100:50:30:6)	DOX	0.07[1]	N.L.
[4]	HSPC:chol:DSPE-PEG:DSPE-Rh (75:50:3:0.6)	DOX	0.16[1]	N.L.
[4]	DPPC:HSPC:chol:DSPE-PEG:DSPE-Rh (100:50:30:6:1.2)	Calcein	0.06[2]	N.L.
[5]	DPPC:HSPC:chol:DSPE-PEG in mole ratios: 100:50:0:0 100:50:75:0 50:50:50:0 50:50:100:0 100:50:0:3 100:50:0:6 100:50:30:6	DOX	 0.11[1] 0.09[1] 0.05[1] 0.07[1] 0.09[1] 0.13[1] 0.05	N.L.
[6]	DSPC:chol:DSPG:DSPE-PEG in mole ratios: 90:45:10:0 (initial drug:lipid ratio 1:60) 70:35:30:10.2 (initial drug:lipid ratio 1:60) 70:35:30:0 (initial drug:lipid ratio 1:30) 90:45:10:10.9 (initial drug:lipid ratio 1:30) 90:90:10:0 (initial drug:lipid ratio 1:30) 70:70:30:0 (initial drug:lipid ratio 1:60) 90:90:10:14.3 (initial drug:lipid ratio 1:60) 70:70:30:12.8 (initial drug:lipid ratio 1:30) 70:70:30:0 (initial drug:lipid ratio 1:30)	Topotecan	 1.96[3] 1.21[3] 2.52[3] 0.82[3] 1.64[3] 1.57[3] 0.13[3] 4.15[3] 2.57	 9.96 7.27 6.70 2.36 3.76 7.61 0.68 11.44 6.21
[7]	S_{100}PC:chol (90:10) S_{100}PC:chol:DSPE-PEG (90:10:5)	Paclitaxel	$7.61\times(10^{-3})$[3,4] $5.10\times(10^{-3})$[3,4]	61.02 57.44
[8]	SPC:chol (80:10) sized to: 530 nm 400 nm 320 nm 180 nm	TFu	 0.27[5] 0.27[5] 0.26[5] 0.24	 88.5 88.7 85.6 80.0
[9]	DPPC:POPC:DPPG:chol:DSPE-PEG (10:10:2:2:2) DPPC:POPC:DPPG:chol:DSPE-PEG-APRPG (10:10:2:2:2)	SU1498	N.L. N.L.	74.6 78.7
[10]	DPPC:chol:DSPE-PEG (18.5:10:1.5) DPPC:chol:DSPE-PEG:DSPE-PEG-maleimide (18.5:10:0.75:0.75)	ZD6126	0.18[6]	19

Table 3. Abbreviations (in order of appearance): HSPC, hydrogenated soy phosphatidylcholine; chol, cholesterol; DOX, doxorubicin; N.L., not listed; DSPE-Rh, N-(lissamine Rhodamine B sulfonyl)-1,2-distearoyl-*sn*-glycero-3-phosphatidylethanolamine; DSPC, 1,2-distearoyl-*sn*-glycero-3-phosphatidylcholine; DPPG, 1,2-dipalmitoyl-*sn*-glycero-3-phosphatidylglycerol; S_{100}PC, soybean PC; SPC, soy PC; TFu, N^3-O-toluyl-5-fluorouracyl; POPC, 1-palmitoyl-2-oleoyl-*sn*-glycero-3- phosphatidylcholine; APRPG, Ala-Pro-Arg-Pro-Ala peptide; SU1498, (E)-3-(3,5-di-isopropyl-4-hydroxyphenyl)-2-[(3-phenyl-*n*-propyl)aminocarbonyl]acrylonitrile, an inhibitor of VEGFR2 tyrosine kinase; ZD6126, N-[(5S)-6,7-dihydro-9,10,11-trimethoxy-3-(phosphonooxy)-5H-dibenzo[a,c]cyclohepten-5-yl]acetamide, a water-soluble prodrug of the tubulin binding agent ZD6126-phenol (N-acetylcolchinol). Where applicable, drug:lipid ratios were calculated based on a [1]DOX MW of 543.53 g·mol^{-1}, a [2]calcein MW of 662.54 g·mol^{-1}, a [3]topotecan MW of 457.92 g·mol^{-1}, a [3]DSPC MW of 790.16 g·mol^{-1}, a [3]DPPG MW of 744.96 g·mol^{-1}, a [3]DSPE-PEG2000 MW of 2805.5 g·mol^{-1}, a [4]S_{100}PC MW of 758.07 g·mol^{-1}, a [4]paclitaxel MW of 853.9 g·mol^{-1}, a [5]TFu MW of 248 g·mol^{-1}, and a [6]ZD6126 MW of 425.37 g·mol^{-1}. *Drug:lipid ratio calculated on the basis of weight: 3.92 mg DOX / 20 mg lipid. All liposomal formulations were prepared by the lipid film hydration technique.

REFERENCES

1. S. Udenfriend, S. Stein, P. Böhlen, W. Dairman, W. Leimgruber, M. Weigele, Fluorescamine: a reagent for assay of amino acids, peptides, proteins, and primary amines in the picomole range, Science 178(63) (1972) 871-872.
2. D.J. Smithies, M.J. van Gemert, M.K. Hansen, T.E. Milner, J.S. Nelson, Three-dimensional reconstruction of port wine stain vascular anatomy from serial histological sections, Phys. Med. Biol. 42(9) (1997) 1843-1847.
3. C. Upson, T. Faulhaber, D. Kamins, D. Laidlaw, D. Schlegel, J. Vroom, R. Gurwitz, A. van Dam, The application visualization system – a computational environment for scientific visualization, IEEE Comput. Graph. Applic. 9 (1989) 30-42.
4. M.H. Gaber, N.Z. Wu, K. Hong, S.K. Huang, M.W. Dewhirst, D. Papahadjopoulos, Thermosensitive liposomes: extravasation and release of contents in tumor microvascular networks, Int. J. Radiat. Oncol. Biol. Phys. 36(5) (1996) 1177-1187.
5. M.H. Gaber, K. Hong, S.K. Huang, D. Papahadjopoulos, Thermosensitive sterically stabilized liposomes: formulation and in vitro studies on mechanism of doxorubicin release by bovine serum and human plasma, Pharm. Res. 12(10) (1995) 1407-1416.
6. S. Dadashzadeh, A.M. Vali, M. Rezaie, The effect of PEG coating on in vitro cytotoxicity and in vivo disposition of topotecan loaded liposomes in rats, Int. J. Pharm. 353(1-2) (2008) 251-259.
7. T. Yang, F.D. Cui, M.K. Choi, J.W. Cho, S.J. Chung, C.K. Shim, D.D. Kim, Enhanced solubility and stability of PEGylated liposomal paclitaxel: in vitro and in vivo evaluation, Int. J. Pharm. 338(1-2) (2007) 317-326.
8. W. Sun, W. Zou, G. Huang, A. Li, N. Zhang, Pharmacokinetics and targeting property of TFu-loaded liposomes with different sizes after intravenous and oral administration, J. Drug Target. 16(5) (2008) 357-365.
9. Y. Katanasaka, T. Ida, T. Asai, N. Maeda, N. Oku, Effective delivery of an angiogenesis inhibitor by neovessel-targeted liposomes, Int. J. Pharm. 360(1-2) (2008) 219-224.
10. M.H. Fens, K.J. Hill, J. Issa, S.E. Ashton, F.R. Westwood, D.C. Blakey, G. Storm, A.J. Ryan, R.M. Schiffelers, Liposomal encapsulation enhances the antitumour efficacy of the vascular disrupting agent ZD6126 in murine B16.F10 melanoma, Br. J. Cancer. 2008 [Epub ahead of print].